DOI: https://doi.org/10.1063/5.0156459

REVIEW ARTICLE | AUGUST 07 2023

Synchronization stability and multi-timescale analysis of renewable-dominated power systems

Special Collection: Nonlinear dynamics, synchronization and networks: Dedicated to Jürgen Kurths' 70th birthday

Rui Ma ; Yayao Zhang ; Miao Han; Jürgen Kurths ; Meng Zhan

Chaos 33, 082101 (2023)
https://doi.org/10.1063/5.0156459

Chaos REVIEW pubs.aip.org/aip/cha

Synchronization stability and multi-timescale analysis of renewable-dominated power systems

Cite as: Chaos 33, 082101 (2023); doi: 10.1063/5.0156459
Submitted: 29 April 2023 · Accepted: 20 July 2023 ·
Published Online: 7 August 2023

View Online Export Citation CrossMark

Rui Ma,[1] Yayao Zhang,[1] Miao Han,[1] Jürgen Kurths,[2,3] and Meng Zhan[1,a)]

AFFILIATIONS

[1]State Key Laboratory of Advanced Electromagnetic Engineering and Technology, Hubei Electric Power Security and High Efficiency Key Laboratory, School of Electrical and Electronic Engineering, Huazhong University of Science and Technology, Wuhan 430074, China
[2]Potsdam Institute for Climate Impact Research, Potsdam 14473, Germany
[3]Institute of Physics, Humboldt University Berlin, Berlin 12489, Germany

Note: This paper is part of the Focus Issue on Nonlinear dynamics, synchronization and networks: Dedicated to Juergen Kurths' 70th birthday.

[a)]**Author to whom correspondence should be addressed:** zhanmeng@hust.edu.cn

ABSTRACT

Synchronization is one of the key issues in three-phase AC power systems. Its characteristics have been dramatically changed with the large-scale integration of power-electronic-based renewable energy, mainly including a permanent magnetic synchronous generator (PMSG) and a double-fed induction generator (DFIG) for wind energy and a photovoltaic (PV) generator for solar energy. In this paper, we review recent progresses on the synchronization stability and multi-timescale properties of the renewable-dominated power system (RDPS), from nodes and network perspectives. All PMSG, DFIG, and PV are studied. In the traditional synchronous generator (SG) dominated power system, its dynamics can be described by the differential–algebraic equations (DAEs), where the dynamic apparatuses are modeled by differential equations and the stationary networks are described by algebraic equations. Unlike the single electromechanical timescale and DAE description for the SG-dominated power system, the RDPS dynamics should be described by the multiscale dynamics of both nodes and networks. For three different timescales, including the AC current control, DC voltage control, and rotor electromechanical timescales, their corresponding models are well established. In addition, for the multiscale network dynamics, the dynamical network within the AC current control timescale, which should be described by differential equations, can also be simplified as algebraic equations. Thus, the RDPS dynamics can be put into a similar DAE diagram for each timescale to the traditional power system dynamics, with which most of power electrical engineers are familiar. It is also found that the phase-locked loop for synchronization plays a crucial role in the whole system dynamics. The differences in the synchronization and multiscale characteristics between the traditional power system and the RDPS are well uncovered and summarized. Therefore, the merit of this paper is to establish a basic physical picture for the stability mechanism in the RDPS, which still lacks systematic studies and is controversial in the field of electrical power engineering.

With the continuous-increasing integration of large-scale renewable energy resources in modern power grids, synchronous generators (SGs) are being replaced by renewable sources enabled by the power electronics technology, and, thus, traditional SG-dominated power system is being gradually transformed into a renewable-dominated power system (RDPS). It is generally regarded as the second revolution of the power system, which will bring changes in all aspects of the power system, including analysis, protection, control, and operation. The traditional power system operation and control relying on the dynamic performance of SG faces a potential failure risk. Accordingly, correct cognition of renewable apparatuses becomes the first and most important aspect. For the SG, its electromechanical dynamics is well described by the classical swing equation (with the same form as the second-order Kuramoto phase oscillator model), showing the rotor motion under power imbalance on the rotor. Different from this simple physical picture, renewable apparatuses highly rely on different negative-feedback controllers under multi-timescale cascade vector controls. The corresponding power imbalance objects are usually separated into the AC

filter inductor, DC-link capacitor, and rotor (if wind power is considered). In addition, the synchronization function is now described by the phase-locking loop technique. So far, the synchronization mechanism underlying the RDPS remains unsolved. In 2021, the China Association for Science and Technology proposed ten key frontier scientific problems, among them: What are the path optimization and stability mechanism of the RDPS? This paper attempts to clarify the synchronization and multiscale properties of the RDPS from nodes and network perspectives by each timescale study separately. Therefore, it uncovers the organization rules of the RDPS dynamics preliminarily. In addition, it makes a close connection between synchronization stability in power systems and phase synchronization in nonlinear sciences.

I. INTRODUCTION

Synchronization has been believed as the source of the spontaneous order of our universe[1] and it has been widely discovered in nature and utilized in engineering, such as biological rhythm, neural systems, social networks, and power grids.[2–6] It has become one of the central problems in many multidisciplinary fields. Power system synchronization stability has been defined by Kundur in his famous textbook, *Power System Stability and Control*: Power system stability may be broadly defined as that property of a power system that enables it to remain in a state of operating equilibrium under normal operating conditions and to regain an acceptable state of equilibrium after being subjected to a disturbance.[7] Usually, it contains two different problems,[7–10] including small-disturbance synchronization stability, for which the disturbance is small and the system can be linearly analyzed, and large-disturbance synchronization stability (also called transient stability) for which a variety of large-disturbance or faults have to be studied and the system nonlinearity has to be considered. Therefore, for proper energy conversion and allocation in the three-phase AC power system, synchronization between any grid-tied apparatuses is an indispensable prerequisite. It is one of the central problems for stable system operation, and it has also attracted much interest of researchers from complex system theory.[11–15]

In traditional power systems, the synchronous generators (SGs) are dominant sources and their dynamic performance largely determines the system dynamics.[7–9] In the past 100 years, the dynamic performance of the SG and further the power system have been well-matured. Different order models of SG with different complexities have been developed to accommodate various application scenarios. Among them, the rotor motion of SG plays a central role within the electromechanical timescale (about 1 s). It is driven by the power imbalance between the input mechanical power and the output electromagnetic power, which is well described by the classical swing equation and is also called as the second-order Kuramoto phase oscillator model in mathematics.[11–18] As the transient stability assessment is conducted as often as every 5 min for checking the ability of the rotor angles of major SGs to maintain synchronization when subjected to a large disturbance, such as lightning, loss of loads or SGs, and three-phase short-circuit faults, it spends a large amount of computational resource. So far, many theoretical methods have been developed.[19–22] For instance, for the single SG infinite bus system, the equal area criterion offers a simple physical picture. For multi-generator systems, some so-called direct methods based on the Lyapunov energy function have been proposed, such as the extended equal area criterion, the potential energy boundary surface method, etc.[19–22]

With the continuous-increasing integration of renewable energy, many SGs are being replaced by the renewable apparatuses with the power electronics technology. Among them, the wind and solar energies are dominant, whose apparatus account for more than half of the total global installed renewable energy capacity.[23,24] Currently, the wind energy is converted to electricity mainly by the double-fed induction generator (DFIG) and permanent magnetic synchronous generator (PMSG). For the solar energy, the photovoltaic (PV) technique is used. Different from the SG, all three dominant renewable apparatuses, including the DFIG, PMSG, and PV, are regulated by multi-timescale cascading vector controls.[25] Usually for the different controlled targets, the AC filter inductor, the DC-link capacitor, and the rotor, they can be separated into the AC current control, DC voltage control (DVC), and rotor electromechanical timescales correspondingly. The current control timescale is the fastest (around 10 ms), which consists of the dynamics of alternating current control (ACC) and line inductor.[26] Within the voltage control timescale, the DC voltage control (DVC), terminal voltage control (TVC), and DC capacitor dynamics are dominant (around 100 ms).[27] Both the current and voltage control dynamics belong to the electromagnetic timescale. In contrast, for the rotor electromechanical timescale, it mainly includes the dynamics of rotor and some associated controls, which is the slowest (around 1 s).[28–30] Therefore, for the RDPS, the system structure and the associated dynamics have become much more complicated. Worse, all renewable apparatuses are protected by sequential switching controls and hardware circuits during severe faults, which could considerably complicate the system dynamic response.[31] Because of these intrinsic properties, it becomes challenging to uncover the working rule for the RDPS dynamics.

The RDPS dynamics has been widely investigated in the academia and industry of electrical power engineering recently.[32–37] It is generally accepted that within the electromagnetic timescale, renewable apparatuses can be simplified as a grid-tied voltage source converter (VSC), and, thus, the converter control performance is crucial.[38–41] Recently, the converter-driven stability has been added as a new stability class by the IEEE task force.[42] Until now, various nonlinear techniques have been used to uncover the transient synchronous stability of the single VSC, e.g., bifurcation analysis, phase portrait, basin of attraction, and numerical analytical methods.[43–45] A simplest second-order model was proposed by focusing the phase-locked loop (PLL) dynamics of the VSC, and it was referred to as the generalized swing equation to show its similarity with the swing equation.[46,47] Based on this low-order model, several other methods have been developed, including the energy function (or Lyapunov function) method, equal area criterion, sum of squares programming, etc.[46–55] On the other hand, synchronization in multi-VSC systems and the VSC with SG have been studied recently.[56–60] The concept of synchronization with 100% renewable energy has also been proposed.[61–63] Clearly, most of these works are restricted to the converter-driven synchronous stability within the electromagnetic timescale and more general synchronous stability of renewable energy apparatuses within the electromechanical timescale has been rarely studied.[64] *Therefore, the organization rule of the RDPS dynamics for different renewable apparatuses within different timescales remains obscure.*

As the SG rotor motion frequency deviation in the traditional power system away from the fundamental frequency (50 or 60 Hz) is relatively small even in the transient process, the phasor technique for sinusoidal steady-state circuit analysis can still be used. Under this so-called quasi-steady state assumption, the electrical network can be described by the nodal admittance matrix. Thus, the differential–algebraic equation (DAE) description, including differential equations for the dynamic apparatus and algebraic equations for the stationary network constitutes the model basis for the traditional stability analysis. With this picture, the system complexity has been greatly reduced. In the RDPS, however, due to the fast dynamics of converters, such as the AC current controller, the quasi-steady state approximation is no longer appropriate. It is generally believed that all-system-level electromagnetic transient (EMT) simulations incorporating the differential dynamics of inductor and capacitor of transmission line are needed. This becomes even more necessary in high-frequency oscillation analysis.[65] For low-frequency one, however, it was also found that the quasi-steady state assumption is still applicable.[66–70] *Therefore, the organization rule of the RDPS dynamics for the network within different timescales remains unclear.*

Clearly, there are many basic problems in the global energy transition for a sustainable and green society. In contrast to a lot of research efforts devoted to the area of small-disturbance stability analysis of the RDPS, this paper attempts to review recent progress on the multi-scale nonlinear modeling and transient synchronization stability analysis. Three typical renewable energy apparatuses, including the PMSG, DFIG, and PV under both electromagnetic and electromechanical timescales, will be discussed here. Not only node but also network performances within each timescale will be explored. The major objective of this review is to uncover the RDPS synchronization stability mechanism. The other objective is to introduce these emerging challenges in our modern electrical power engineering to researchers of nonlinear complex systems and expect to stimulate trans-disciplinary interest. The whole paper is organized as follows. The multi-scale characteristics of node and network dynamics are introduced in Secs. II and III, respectively, including the PMSG, DFIG, and PV systems. All three timescales, including the AC current control, DC voltage control, and rotor timescales, will be studied. The conclusions are addressed in Sec. IV. Finally, challenges and research trends are discussed in Sec. V.

II. MULTI-TIMESCALE NODE DYNAMICS

Among various types of renewable energy generation, the most common are the permanent magnet synchronous generator, double-fed induction machine, and photovoltaic, whose major control structures are shown in Figs. 1–3, respectively. Generally, the electrical systems are composed of two parts, including a machine-side converter (MSC) and a grid-side converter (GSC), which are connected by a DC-link capacitor.

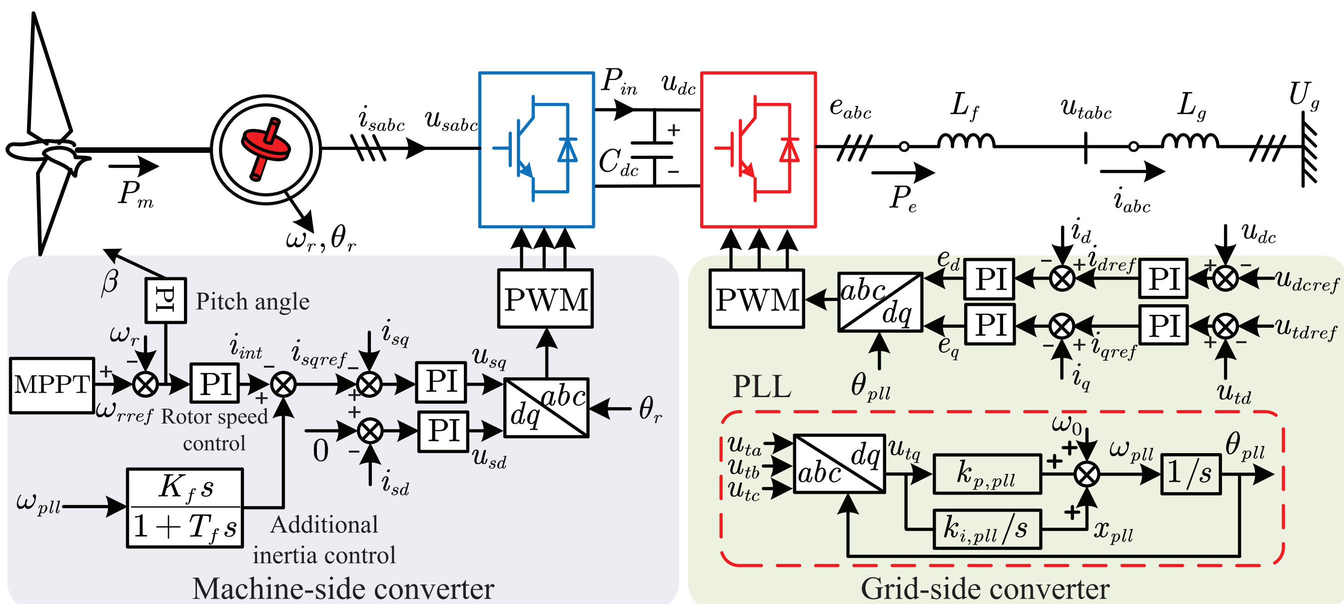

FIG. 1. Main control structures of a typical PMSG system. On the machine side, the machine-side converter (MSC) usually employs the pitch angle control, maximum power point tracking (MPPT), additional inertia control (AIC), rotor speed control (RSC), and alternating current control (ACC). On the grid side, the grid-side converter (GSC) uses the direct voltage control (DVC), terminal voltage control (TVC), phase-locked loop (PLL), and ACC. The MSC and GSC are physically separated and solely connected by a DC-link capacitor C_{dc}. Usually, the PLL is used for grid synchronization.

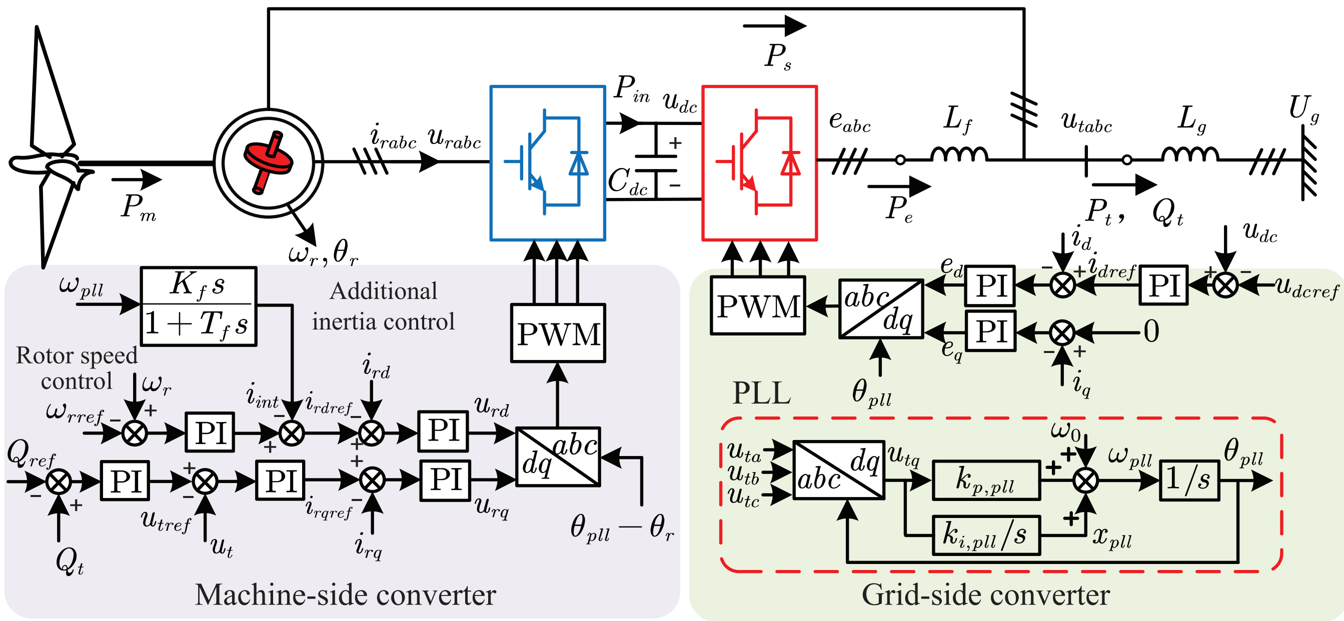

FIG. 2. Main control structures of a typical DFIG system. Different from the PMSG, the stator of the induction generator of the DFIG is directly tied to the grid, while its rotor is connected through the machine-side converter (MSC) and grid-side converter (GSC). In addition to the pitch angle control and the maximum power point tracking (MPPT) control, the MSC consists of the additional inertia control (AIC), rotor speed control (RSC), reactive power control (RPC), terminal voltage control (TVC), and alternating current control (ACC). The controllers of the GSC are similar to those of the PMSG in Fig. 1. In addition, the total power P_t generated by the DFIG is composed of P_e through the GSC and P_s through the stator of the induction generator.

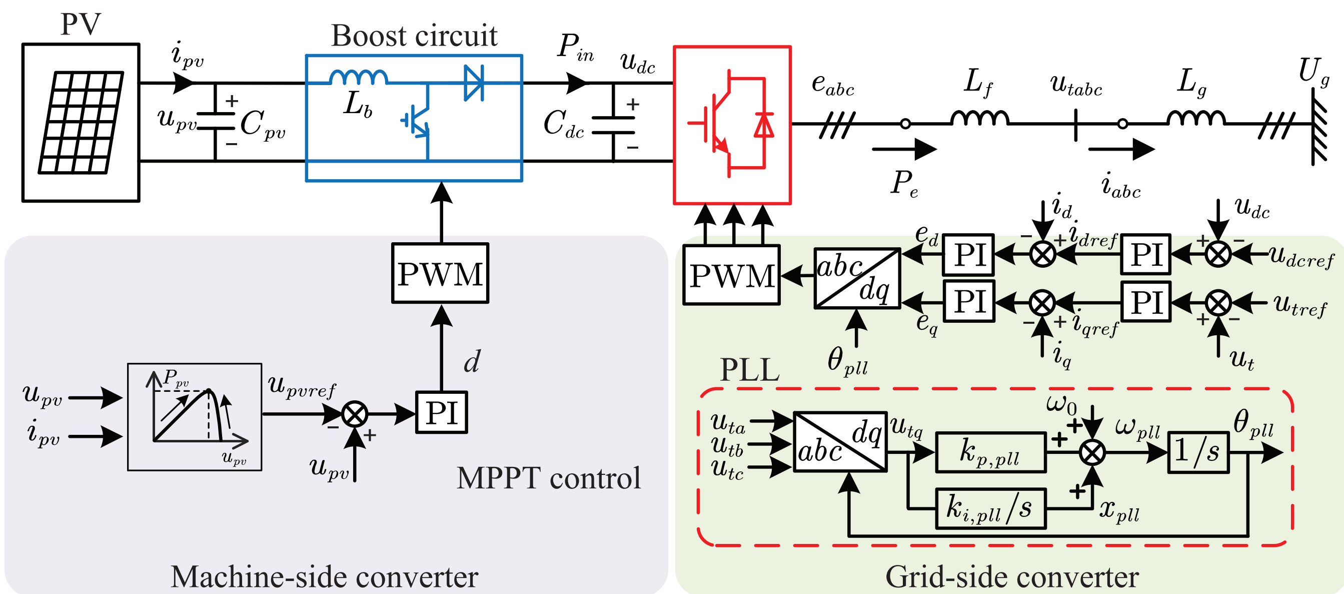

FIG. 3. Main control structures of a typical PV system. Again, the GSC is similar. For the MSC, the PV panels use a DC–DC boost circuit to regulate its output voltage u_{pv} for the maximum power. Here, d denotes the step-up ratio. The maximum power of P_{pv} is determined by the PV characteristic curve, which is a nonlinear function of the output voltage u_{pv}. $P_{pv} = u_{pv} i_{pv}$. Different from the PMSG and DFIG for the wind energy, there is no rotation component, and, thus, it has only electromagnetic timescale dynamics.

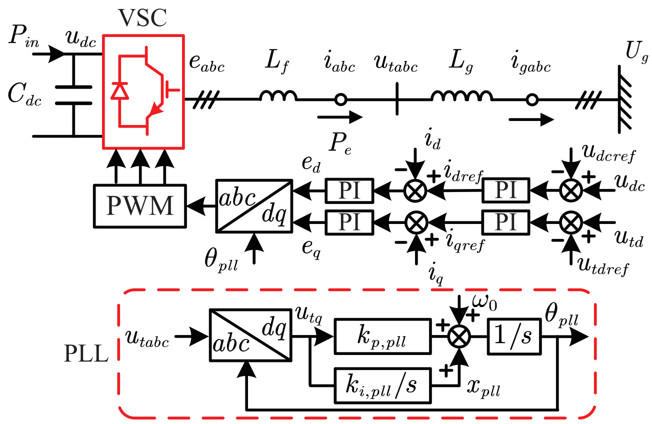

FIG. 4. A typical grid-tied VSC and its control structures, which can be well separated from any grid-tied renewable apparatuses, including the PMSG, DFIG, and PV. The VSC applies the electromagnetic timescale cascading controllers, including the outer controllers (e.g., the DVC and TVC) and the inner ACC controllers. Usually, the PLL is used for the grid synchronization, by inputting u_{tabc} and outputting θ_{pll}. With θ_{pll}, the PLL dq rotating coordinate can be established. Within the electromagnetic timescale, P_{in}=constant is usually assumed.

On the grid side, the GSC is integrated into the grid via a filter inductor L_f and an equivalent grid inductor L_g. The GSC typically applies multi-timescale cascading vector controllers, including the ACC, the DVC, and the PLL. To emphasize the importance of the GSC, its control structure has been separated and shown in Fig. 4. The corresponding coordinate frames and variables in the PLL control are shown in Fig. 5, where φ_{pll} denotes the phase difference between xy and the PLL dq frames, $\varphi_{pll} = \theta_{pll} - \omega_0 t$, and $\omega_{pll} = \dot{\theta}_{pll} = \dot{\varphi}_{pll} + \omega_0$. The angular frequency ω_0 refers to the fundamental frequency of the power grid. Detailed definitions of variables can be found in Appendix A. The aim of the PLL is to track the angle of the terminal voltage and maintain synchronization with the grid.

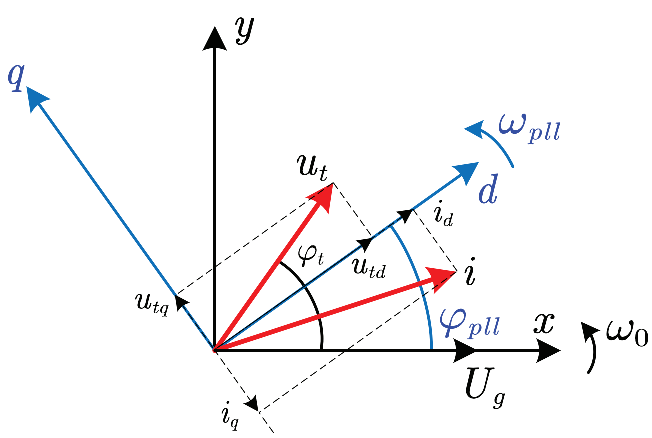

FIG. 5. Schematic showing variables in the common synchronous rotating xy frame and the PLL dq frame used in the GSC.

It inputs three-phase AC terminal voltages: u_{ta}, u_{tb}, u_{tc}, and outputs a phase θ_{pll}, which is further used for vector controls within the PLL dq rotating coordinate. Therefore, for a perfect synchronization or in the steady state, the q-axis component of the AC terminal voltage u_{tq} is equal to 0 based on the PLL control structure in Fig. 1. Correspondingly, the d-axis component of the terminal voltage u_{td} equals the amplitude of the terminal voltage U_t as $U_t = \sqrt{u_{td}^2 + u_{tq}^2}$. In the meantime, the output frequency of the PLL ω_{pll} is the fundamental frequency ω_0 (or the synchronous frequency).[26,37,71] To maintain the DC voltage, the DVC governs the d-axis current reference i_{dref}, and correspondingly to maintain the terminal voltage amplitude, the TVC regulates the q-axis current reference i_{qref}. Based on these two current references (i_{dref} and i_{qref}), the ACC further generates the internal voltages references (e_d and e_q) in the same dq coordinate provided by the PLL. By the pulse-width modulation (PWM) technique, six insulated gate bipolar translators are driven by the modulated signals of reference voltages to produce the converter output voltages e_{abc}. To make these cascade controllers work properly, usually the inner ACC has the fastest response around 10 ms, and the outer voltage controllers (i.e., the DVC and the TVC) have a medium time constant of around 100 ms. In addition, the classical proportional-integral (PI) negative-feedback control with the proportional coefficient k_p and integral coefficient k_i has been widely used.[72,73]

On the machine side, for the wind power, usually the controller dynamics is much slower with a time constant of about 1 s and belongs to the electromechanical timescale. The MSC uses a similar cascade vector control strategy. However, the PMSG uses a SG, the DFIG uses an (asynchronous) induction generator, and the PV has no rotating component. Therefore, their controls are different. These details will be introduced later.

Usually the control target of the GSC is to realize synchronization with the grid, plus a stable terminal voltage and a stable DC voltage on the capacitor. In contrast, that of the MSC is to make the power conversion efficiently, namely, the maximum power tracking, active and reactive power controls, etc. Therefore, as the first step in studying the renewable energy apparatus, we will study its grid-tied converter, by neglecting all the machine-side dynamics and assuming that the injection power from the machine side, P_{in}, is constant, as illustrated in Fig. 4. Thus, we will study the electromagnetic timescale dynamics (including the current and voltage control timescale dynamics) of the GSC in Fig. 4 first, and then the machine-side dynamics of the MSC for all three major renewable apparatuses in Figs. 1–3.

A. Current control timescale dynamics

In Fig. 4 for a single-VSC grid-tied system, within the current timescale, all outer controllers, including the DVC and the TVC can be ignored and the current references i_{dref} and i_{qref} can be treated as constants (or tunable parameters). However, the dynamics of the ACC, the filter inductor, and the transmission line should be considered.

The dynamics of the PLL is modeled as

$$\begin{cases} \dot{\varphi}_{pll} = x_{pll} + k_{p,pll} u_{tq}, \\ \dot{x}_{pll} = k_{i,pll} u_{tq}, \end{cases} \tag{1}$$

and the dynamics of the integration parts of the ACC is modeled as

$$\begin{cases} \dot{x}_{acc1} = k_{i,acc}(i_{dref} - i_d), \\ \dot{x}_{acc2} = k_{i,acc}(i_{qref} - i_q), \end{cases} \tag{2}$$

with the internal voltages e_{dq} generated by the ACC given by

$$\begin{cases} e_d = k_{p,acc}(i_{dref} - i_d) + x_{acc1}, \\ e_q = k_{p,acc}(i_{qref} - i_q) + x_{acc2}. \end{cases} \tag{3}$$

Meanwhile, all voltage and current vectors in the local dq PLL synchronous frame and the xy common synchronous frame can be transferred to each other by the rotating transformation, as illustrated in Fig. 5. For example, for the internal voltages (e_{xy} or e_{dq}), we have

$$\begin{bmatrix} e_x \\ e_y \end{bmatrix} = \begin{bmatrix} \cos\varphi_{pll} & -\sin\varphi_{pll} \\ \sin\varphi_{pll} & \cos\varphi_{pll} \end{bmatrix} \begin{bmatrix} e_d \\ e_q \end{bmatrix}, \quad \begin{bmatrix} e_d \\ e_q \end{bmatrix} = \begin{bmatrix} \cos\varphi_{pll} & \sin\varphi_{pll} \\ -\sin\varphi_{pll} & \cos\varphi_{pll} \end{bmatrix} \begin{bmatrix} e_x \\ e_y \end{bmatrix}. \tag{4}$$

In the single-VSC system in Fig. 4, the VSC integrates to the grid by a filter inductor L_f, and the corresponding currents on the filter inductor (i_{xy}) are determined by the differential equations, namely,

$$\begin{cases} \dot{i}_x = \dfrac{\omega_0}{L_f} e_x - \dfrac{\omega_0}{L_f} u_{tx} + \omega_0 i_y, \\ \dot{i}_y = \dfrac{\omega_0}{L_f} e_y - \dfrac{\omega_0}{L_f} u_{ty} - \omega_0 i_x, \end{cases} \tag{5}$$

and meanwhile, the currents i_{gxy} on the grid inductor L_g satisfy the following differential equations:

$$\begin{cases} \dot{i}_{gx} = \dfrac{\omega_0}{L_g} u_{tx} - \dfrac{\omega_0}{L_f} u_{gx} + \omega_0 i_{gy}, \\ \dot{i}_{gy} = \dfrac{\omega_0}{L_g} u_{ty} - \dfrac{\omega_0}{L_f} u_{gy} - \omega_0 i_{gx}. \end{cases} \tag{6}$$

Considering Eqs. (5) and (6) and $i_x = i_{gx}$ and $i_y = i_{gy}$, we obtain that the terminal voltages u_{txy} can be written as a function of the internal voltages e_{xy} and the grid voltages u_{gxy}, i.e.,

$$\begin{cases} u_{tx} = \dfrac{L_g}{L_f + L_g} e_x + \dfrac{L_f}{L_f + L_g} u_{gx}, \\ u_{ty} = \dfrac{L_g}{L_f + L_g} e_y + \dfrac{L_f}{L_f + L_g} u_{gy}. \end{cases} \tag{7}$$

Therefore, with the combined filter inductor dynamics in Eq. (5), the VSC dynamics in Eqs. (1) and (2), the coordinate transformations in Eqs. (4), and ($u_{gx} = U_g$ and $u_{gy} = 0$), we have the whole DAEs for the single-VSC-infinite-bus system within the current control timescale in Fig. 4. The model details and its bifurcation and dynamical analysis results can be found in Ref. 26. Some other works on the current timescale dynamics are represented in Refs. 44, 74, and 75. The model can also be easily extended to include slower dynamical components. More discussions on the network part will be given later.

B. Voltage control timescale dynamics

Since in a very recent paper, we have already reviewed the models of grid-tied converters within the voltage control timescale, we give here only the main idea and results.[35] Within this timescale, the outer controllers and the PLL become our target. Since their dynamic responses are comparatively slower than that of the ACC,[44,76,77] all ACC dynamics can be ignored by assuming that the output currents instantaneously track their references, i.e., $i_d = i_{dref}$, and $i_q = i_{qref}$.

For the simplest case, in the low voltage ride through, we may even freeze all voltage controllers and set constant current references, i.e., i_{dref}=constant, and i_{qref}=constant. Under this simplification, it is reasonable to have the following simplest second-order model:

$$M_{eq}\ddot{\varphi}_{pll} = P_{meq} - P_{eq} - D_{eq}\left(\varphi_{pll}\right)\dot{\varphi}_{pll}, \tag{8}$$

where

$$\begin{cases} M_{eq} = \dfrac{1 - k_{p,pll} L_g i_{dref}}{k_{i,pll}}, \\ P_{meq} = \omega_0 L_g i_{dref}, \\ P_{eq} = U_g \sin\varphi_{pll}, \\ D_{eq} = \dfrac{k_{p,pll}}{k_{i,pll}} U_g \cos\varphi_{pll} - L_g i_{dref}. \end{cases} \tag{9}$$

Here, M_{eq}, P_{meq}, P_{eq}, and D_{eq} represent the equivalent inertia, mechanical power, electromagnetic power, and damping coefficient, respectively.

Since the second-order model in Eq. (8) considers the PLL dynamics solely and shows a certain similarity with the classical swing equation[7–9] (i.e., $M\ddot{\varphi} = P_m - P_e - D\dot{\varphi}$), it has been referred to as the generalized swing equation, for its centrality in the model hierarchical structure. It has also been widely used to study the synchronous stability problems of PLL-based VSC.[46–55]

Note that in the derivation of Eq. (8), we have used the algebraic relation between the terminal voltage $\mathbf{U}_t$ ($\mathbf{U}_t = u_{td} + ju_{tq}$), the infinite bus voltage $\mathbf{U}_g$ ($\mathbf{U}_g = U_g\cos\varphi_{pll} - jU_g\sin\varphi_{pll}$), and the VSC current output $\mathbf{I}_{\mathrm{VSC}}$ ($\mathbf{I}_{\mathrm{VSC}} = i_d + ji_q$). The (differential) dynamics of the filter inductor and the transmission line are ignored, similar to the stability analysis in the traditional power system, but different from what we have done for the current timescale dynamics. The details are

$$\mathbf{U}_t = \mathbf{U}_g + j\omega_{pll} L_g \mathbf{I}_{\mathrm{VSC}} \tag{10}$$

and

$$\begin{cases} u_{td} = -\omega_{pll} L_g i_{qref} + U_g\cos\varphi_{pll}, \\ u_{tq} = \omega_{pll} L_g i_{dref} - U_g \sin\varphi_{pll}. \end{cases} \tag{11}$$

Further, when the active power branch (including the DVC and DC capacitor dynamics) is considered, a fourth-order model is obtained

$$\begin{cases} \dot{\varphi}_{pll} = x_{pll} + k_{p,pll} u_{tq}, \\ \dot{x}_{pll} = k_{i,pll} u_{tq}, \\ \dot{u}_{dc} = \dfrac{1}{C_{dc} u_{dc}} (P_{in} - P_e), \\ \dot{x}_{dvc} = k_{i,dvc}(u_{dc} - u_{dcerf}), \end{cases} \tag{12}$$

where the first two equations denote the PLL dynamics, and the last two equations represent the dynamics of the DC capacitor and the DVC. P_{in} denotes the input power on the DC capacitor, and P_e

represents the electromagnetic output power of the VSC, as shown in Fig. 4. To be compared with the swing equation, which reflects both synchronization and power balance simultaneously, here the synchronization of the VSC is realized by the PLL, and the power balance is achieved by the DVC and the DC capacitor dynamics. In this respect, these fourth-order equations [Eq. (12)] can be referred to as the extended generalized swing equations.[35]

In addition, by considering the TVC dynamics, a fifth-order model can be obtained

$$\begin{cases} \dot{\varphi}_{pll} = x_{pll} + k_{p,pll}u_{tq}, \\ \dot{x}_{pll} = k_{i,pll}u_{tq}, \\ \dot{u}_{dc} = \dfrac{1}{C_{dc}u_{dc}}(P_{in} - P_e), \\ \dot{x}_{dvc} = k_{i,dvc}(u_{dc} - u_{dcerf}), \\ \dot{x}_{tvc} = k_{i,tvc}(u_{td} - u_{tderf}), \end{cases} \tag{13}$$

where the last equation is for the TVC dynamics.

Here, only differential equations are listed and all algebraic equations, including u_{td}, u_{tq}, P_e, i_{dref}, and i_{qref} are not shown. Clearly, the PLL plays a central role in the synchronization dynamics. The organization rule of the synchronization stability of a grid-tied converter within the DC voltage timescale has been well summarized in Ref. 35, where the multiscale dynamics of the VSC are elaborated in the electromagnetic timescale. For some other relevant works and numerical results of the VSC dynamics, see Refs. 44, 71, 78, and 79.

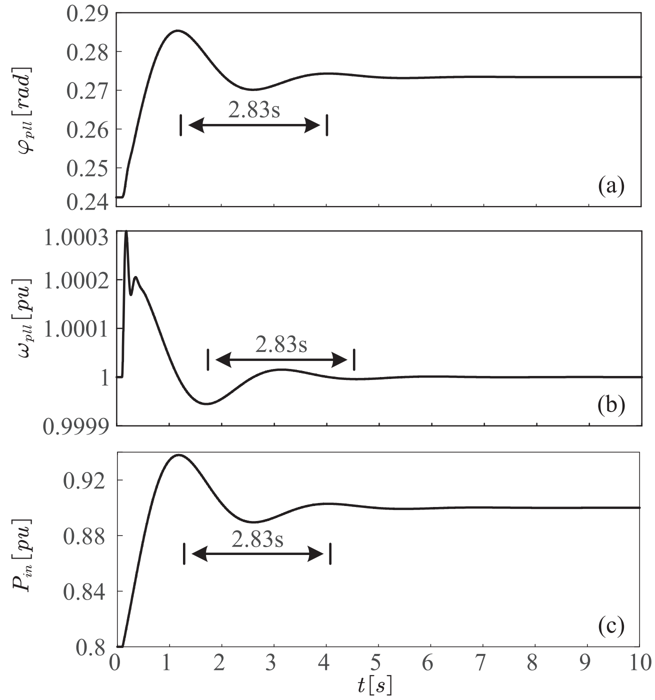

FIG. 6. Time series of (a) the PLL output angle φ_{pll}, (b) the PLL output frequency ω_{pll}, and (c) the injection power from the machine side P_{in} when the PMSG suffers a power variation on the machine side, in the absence of the AIC. Clearly, the system is stable and the three variables oscillate at a low frequency, 0.35 Hz (0.35 Hz $\approx$ 1/2.83 s), indicative of an electromechanical timescale dynamics.

C. Machine-side timescale dynamics

In the above analyses, various models of the grid-tied VSC within the electromagnetic timescale have been studied, all under the assumption that the input mechanical power on the DC capacitor is unchanged, i.e., P_{in}=constant. When the machine-side controls are considered, this equality may be broken. Next, let us shift from the GSC to the MSC. Due to the distinct structures of the MSC of the PMSG, DFIG, and PV, we have to study them individually.

1. Permanent magnetic synchronous generator

The machine-side controls of the PMSG are illustrated in the left part of Fig. 1. Without losing generality, the zero d-axis current control is adopted. The MSC includes the pitch angle control, maximum power point tracking control (MPPT), additional inertia control (AIC), rotor speed control (RSC), and ACC. The MPPT and the pitch angle control regulate the speed and the pitch angle of the wind turbine to capture the maximum wind energy, respectively.[80,81] For the current references of the stator, the q-axis reference i_{sqref} is regulated by both the RSC and the AIC, while the d-axis reference i_{sdref} is set as zero. Based on the current references, the ACC generates the corresponding voltage references u_{sq} and u_{sd} in the rotor frame of the PMSG based on the rotor position θ_r. After a coordinate transformation, trigger signals are produced by the same PWM technology based on the references of u_{sq} and u_{sd}. The MSC and the GSC are separated by a DC-link capacitor C_{dc}. Since the MPPT and pitch angle control are slower than the RSC and AIC, their dynamics can be ignored. Thus, we set P_m = constant in our study. Meanwhile, as the dynamics of the ACC is comparatively faster than those of the RSC and AIC, it can be assumed that the output currents instantaneously track their references, i.e., $i_d = i_{dref}$, and $i_q = i_{qref}$; this is the same as what we have done in the study of the voltage control timescale dynamics for the GSC. Therefore, within the electromechanical timescale, the dynamics of RSC and AIC of the MSC should be dominant, while those of the MPPT, pitch angle controls, and ACC can be ignored. In addition, as we have known that the GSC is mainly within the electromagnetic timescale, its dynamics can also be completely ignored.

Next, let us analyze the dominant dynamical behavior by numerical simulations. As the first case, we consider the PMSG in the absence of the AIC. Under this situation, the MSC has no direct connection with the grid.[82] In Fig. 6, when the system suffers a power variation on the machine side, the input power P_{in} on the capacitor can respond to the disturbance and further transfer it to the GSC. Clearly, P_{in}, φ_{pll}, and ω_{pll} oscillate at 0.35 Hz (0.35 Hz $\approx$ 1/2.83 s) and show the electromechanical timescale character. However, when a grid-side disturbance is considered, for example, when the system suffers a voltage dip on the grid side in Fig. 7, P_{in} remains unchanged and shows no response. In addition, both φ_{pll} and ω_{pll} oscillate faster at 6.25 Hz (6.25 Hz $\approx$ 1/0.16 s), indicative of an electromagnetic timescale dynamics. Therefore, we infer that when the AIC is disabled, the DC capacitor can truly isolate the MSC and the

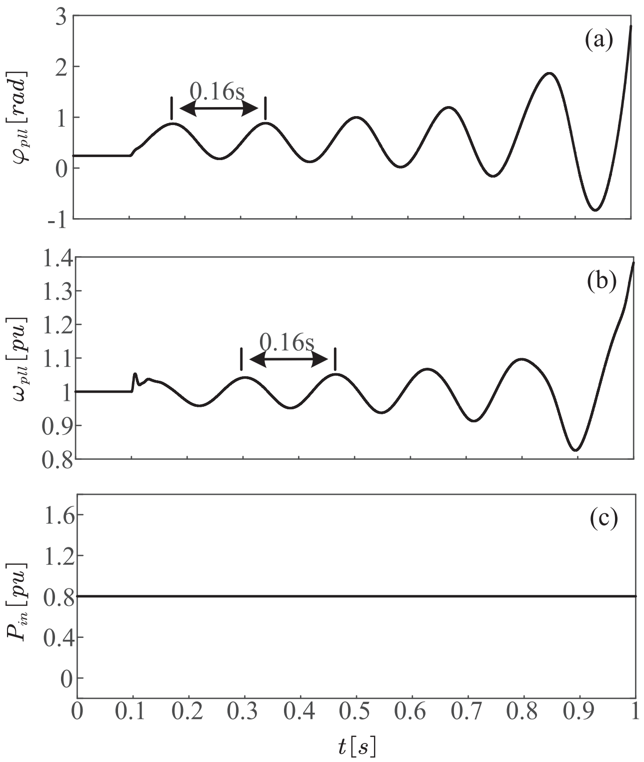

FIG. 7. Similar to Fig. 6, but for a voltage-dip fault on the grid side instead. Now, P_{in} remains a constant, showing that the MSC has no response to the grid disturbance. The system is unstable and both φ_{pll} and ω_{pll} oscillate at a comparatively higher frequency, 6.25 Hz (6.25 Hz $\approx$ 1/0.16 s), indicative of an electromagnetic timescale dynamics.

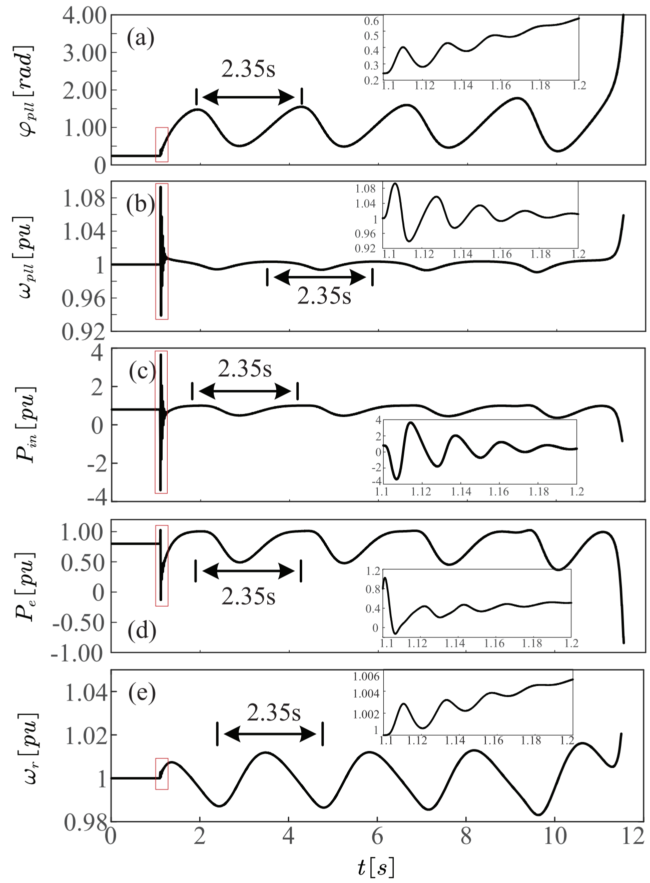

FIG. 8. Time series of (a) the PLL output angle φ_{pll}, (b) the PLL output frequency ω_{pll}, (c) the injection power from the machine side P_{in}, (d) the electromagnetic power output P_e, and (e) the rotor speed ω_r, when the PMSG suffers a voltage-dip fault at 1.1 s. Different from Figs. 6 and 7, the AIC is incorporated. It can be seen that the system becomes unstable and the oscillation frequency is about 0.43 Hz (0.43 Hz $\approx$ 1/2.35 s), falling into the electromechanical timescale. In addition, the EMT dynamics within the short period of the fault occurrence magnified in the insets are apparent.

GSC, and the synchronous stability of the PMSG falls into the electromagnetic timescale category. Therefore, many previous works on the PMSG by focusing on the GSC dynamics are reasonable.[83] Note that all major abbreviations and symbols are listed in Appendix A and all parameters used here are summarized in Appendix B.

For the opposite case, when the AIC is enabled, the input power P_{in} on the capacitor can be partially regulated by the AIC, which relies on the output frequency ω_{pll} of the PLL on the grid side, as shown in Fig. 1.[84,85] Thus, now the MSC and the grid are coupled. As an example, when the infinite bus voltage U_g dips to 0.305 pu at 1.1 s, the time series of the output phase φ_{pll} and frequency ω_{pll} of the PLL are shown in Figs. 8(a) and 8(b), respectively, where their oscillation periods are the same as about 0.43 Hz (0.43 Hz $\approx$ 1/2.35 s) during the fault. Clearly, they exhibit an electromechanical timescale dynamics. For some other variables, the input power P_{in}, the electromagnetic output power P_e, and the rotor frequency ω_r are shown in Figs. 8(c)–8(e), exhibiting similar dynamical behaviors. Apparently, different from the PMSG in the absence the AIC in Fig. 7, here the MSC can clearly respond to the grid-side disturbance. In addition, to show the multi-scale character between the electromagnetic and electromechanical timescales, the electromagnetic dynamics for all variables at the initial stage of the fault around 1.1–1.2 s are magnified and shown in the insets. As shown in Fig. 8, the electromagnetic dynamics are rapidly damped after the fault, and then the variables exhibit the electromechanical behavior.

As the AIC needs the input information of the PLL frequency ω_{pll}, even within the electromechanical timescale, the PLL is important. Hence, for the dominant controllers, we need the AIC and the RSC on the machine side and the PLL on the grid side. Combined with the rotor dynamics, they become dominant. Finally, the control structure of the PMSG within the electromechanical timescale after the simplification is illustrated in Fig. 9. The system leading, slowest timescale is the electromechanical timescale if the AIC is considered. Otherwise, it is the DC voltage control timescale. All these useful results are summarized in Table I.

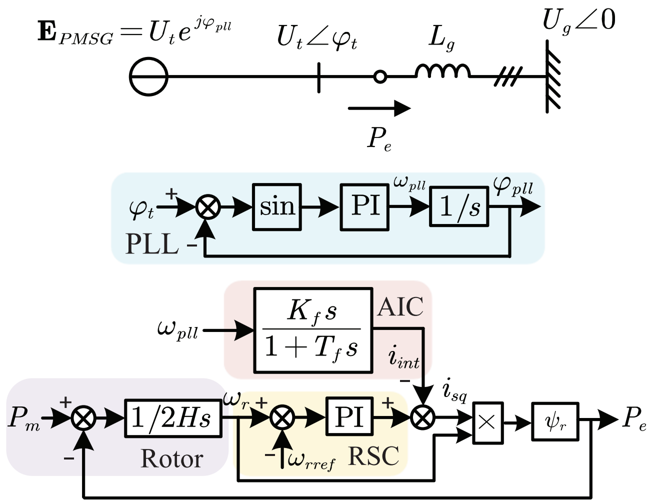

FIG. 9. Simplified structures of the PMSG system with the AIC within the electromechanical timescale. The PMSG can be simplified as a controlled voltage source, whose power output P_e depends on the dynamics of the rotor, the AIC and RSC on the machine side, and the PLL on the grid side. Here, ψ_r denotes the rotor flux-linkage and can be set as a constant.

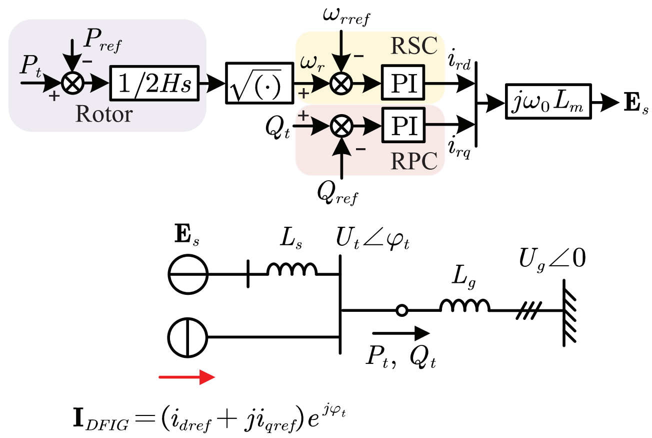

FIG. 10. Simplified structures of the DFIG system within the electromechanical timescale. On the top for the MSC, only the dynamics of rotor, RSC, and the RPC are kept. On the bottom, the whole DFIG can be viewed as a Thevenin branch (i.e., a voltage source in series with an equivalent stator inductor L_s from the MSC and the stator) paralleled with a current source (from the GSC). L_m is the mutual inductance between the stator and rotor.[86]

2. Double-fed induction generator

Different from the PMSG, the stator of the induction generator of the DFIG is directly connected with the grid, while the rotor is connected through the MSC and GSC, as shown in Fig. 2. This is the reason for how the name of DFIG comes. In addition to the pitch angle and the MPPT control, the MSC consists of the AIC, RSC, reactive power control (RPC), TVC, and ACC. Compared with the PMSG, where the DVC and TVC are installed on the grid side, here the MSC adopts the TVC to govern the terminal voltage, and the GSC adopts the DVC to regulate the DC-link voltage.[81] In addition, the totally generated active power P_t to the grid is composed of the slip power P_e (from the rotor and the GSC) and P_s (from the stator). Generally, P_e is less than 20%–30% of the total power P_t.[86,87] In this respect, the converters of the DFIG have lower cost than those of the PMSG. Further, since the MSC regulates the terminal voltage, it has not only a control signal connection with the grid but also the electrical signal connection by the excitation of the induction generator. Therefore, in contrast to the PMSG, the DFIG always performs electromechanical timescale dynamics for either the AIC considered or not.

As now the dynamics of the DC capacitor can be neglected, the DFIG system can be simplified and separated into two parts, as shown in Fig. 10, including the GSC part and the induction generator part along with the MSC. Within the electromechanical timescale, the induction generator part can be simplified as a controlled voltage source in series with a stator inductor L_s, as shown the top of Fig. 10. Based on the algebraic equations of the flux-linkage of the induction generator,[86] the voltage of the induction generator $\mathbf{E}_s$ can be simplified as $j\omega_0 L_m \mathbf{I}_r$, where L_m denotes the (constant) mutual inductance between the stator and rotor, and $\mathbf{I}_r$ represents the rotor current ($\mathbf{I}_r = i_{rd} + j i_{rq}$). It is regulated by the rotor dynamics and machine-side controls, including the AIC, RSC, and RPC. For the GSC part, it is composed of the DC capacitor dynamics, DVC, and ACC. Similar to the grid-tied VSC, it can be treated as a static current source within the present electromechanical timescale. As a result, the rotor dynamics, RSC, and RPC are dominant. All these useful results are shown in Table I.

TABLE I. Multi-timescale dynamics of nodes.

	Leading slowest timescale	Dominant dynamics
PMSG without AIC	DC voltage control timescale	DVC, TVC, and PLL
PMSG with AIC	Electromechanical timescale	Rotor dynamics, RSC, AIC, and PLL
DFIG	Electromechanical timescale	Rotor dynamics, RSC, and RPC
PV	DC voltage control timescale	MPPT, DVC, TVC, and PLL

3. Photovoltaic system

A double-stage PV generation system is illustrated in Fig. 3, where the PV panels are integrated into the GSC through a DC–DC boost circuit.[88–90] The DC–DC circuit and the MPPT control are used to regulate its output voltage u_{pv} of the PV panel and track the maximum power. The MPPT control governs the step-up ratio d by tracking the voltage reference u_{pvref}. The u_{pvref} is computed based on the MPPT characteristic curve, on which the PV panel power output P_{pv} [$P_{pv} = u_{pv} i_{pv} = f_{pv}(u_{pv})$] is a nonlinear function of u_{pv}.

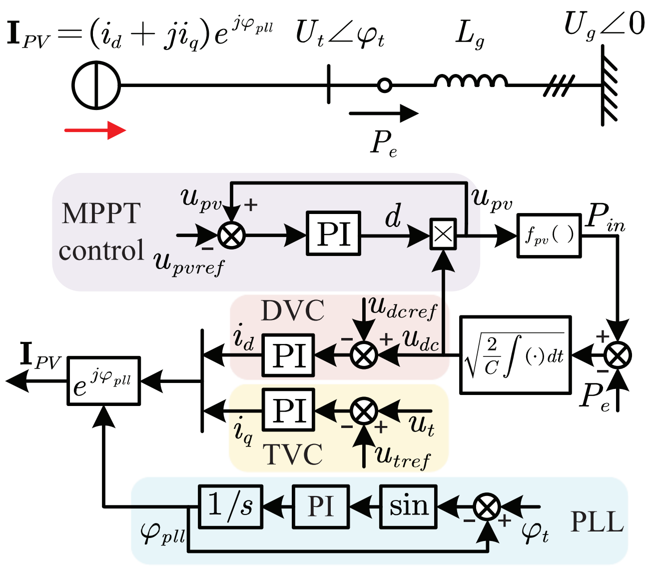

FIG. 11. Simplified structures of the PV system within the DC voltage control timescale. The PV node is simplified as a controlled current source, with the MPPT, DVC, TVC, and PLL included. The f_{pv} is a nonlinear function between P_{pv} ($P_{pv} = u_{pv} i_{pv}$) and u_{pv} in the PV characteristic curve.

It also depends on external environmental temperature and illumination. The other controls of the GSC are the same as those of the typical VSC as shown in Fig. 4. Different from the wind generators, the PV system has no rotation component and no electromechanical timescale dynamics. Thus, the leading slowest timescales of the PV system is the DC voltage control timescale, where the voltage reference u_{pvref} under the long-term variations of temperature and illumination can be set as a constant. Both the PV and the PMSG without the AIC fall into the electromagnetic timescale category and their dynamics are dominated by the GSC. Similar to the VSC, the PV system within the DC voltage control timescale can be simplified as a controlled current source; the simplified model is shown in Fig. 11. However, unlike the VSC in Fig. 4, the input power P_{in} on the capacitor is no longer a constant and it changes with the MPPT control. In this respect, the dynamics of the MPPT, DVC, TVC, and PLL are dominant. These results are added in Table I.

III. MULTI-TIMESCALE NETWORK DYNAMICS

It is well known that in the transient stability analysis of the SG-dominated power system, the system can be well described by DAEs, including differential equations for the dynamic apparatuses and algebraic equations for the stationary network. In this respect, the SG stator flux-linkage transients and its rotor speed variations have been ignored. In addition, the network transients have also been completely neglected. For the details of these model approximation effects, see Ref. 7. In a sharp contrast, for the RDPS, this basic physical picture may change.[66–70] Different from the single-timescale dynamics of the SG, the node multi-timescale dynamics of renewable apparatuses may also drive the network to exhibit multi-timescale character, although the physical apparatus of the AC transmission lines for the network is unchanged.

So far, there are few works focusing on the network dynamics. In one of our recent papers,[66] the dynamic and static networks, which are described by the differential equations and algebraic equations, respectively, are studied and compared. It is found that the frequency range for different behaviors can be divided into three regions, including low-frequency region I (below 10 Hz), resonance region II (from 10 to 200 Hz), and high-frequency region III (above 200 Hz). Only within region I, the difference between the dynamic and quasi-steady networks is tiny, which indicates that the quasi-steady network model is only reasonable for low-frequency studies. For the frequency above 10 Hz, there is a visible difference between these two models, and, thus, the network transients have to be fully considered. More details can be found in Ref. 66. Therefore, the 10 Hz oscillation frequency as a division is critical. Furthermore, based on the facts that the current control, voltage control, and rotor exhibit three different timescales: 100, 10, and 1 Hz, respectively, it is understandable that for the voltage control and electromechanical timescales, we can still use the quasi-steady network model, and oppositely, for the current control timescale, we have to use the dynamic network model.

To compare with the network and node models in the traditional power system better, all important knowledge, such as the Kron reduction of network and the classical model of SG, are given in Appendixes C and D, respectively.

A. Quasi-steady network

First, let us study the quasi-steady network within the DC voltage control and electromechanical timescales. Under these timescales, the renewable apparatus (or grid-tied VSC) works as a controlled current source, accompanying with some other traditional voltage sources (e.g., the infinite bus and SGs) on the network.[66] We have to treat these different types of node separately, namely,

$$\begin{bmatrix}\mathbf{I}_V\\ \mathbf{I}_C\end{bmatrix}=\mathbf{Y}_r\begin{bmatrix}\mathbf{U}_V\\ \mathbf{U}_C\end{bmatrix}, \tag{14}$$

where $\mathbf{I}_V$ and $\mathbf{I}_C$ denote the current vectors of the voltage and current source nodes, respectively, $\mathbf{U}_V$ and $\mathbf{U}_C$ represent the voltage vectors of the voltage and current nodes, respectively, and $\mathbf{Y}_r$ represents the reduced nodal admittance matrix,

$$\mathbf{Y}_r=\begin{bmatrix}\mathbf{Y}_{ma} & \mathbf{Y}_{mb}\\ \mathbf{Y}_{mc} & \mathbf{Y}_{md}\end{bmatrix}. \tag{15}$$

Here, for the network, $\mathbf{I}_C$ and $\mathbf{U}_V$ are inputs from the apparatuses, and $\mathbf{I}_V$ and $\mathbf{U}_C$ are outputs, which should be solved. After some algebraic manipulations, we have

$$\begin{bmatrix}\mathbf{I}_V\\ \mathbf{U}_C\end{bmatrix}=\mathbf{M}\begin{bmatrix}\mathbf{U}_V\\ \mathbf{I}_C\end{bmatrix}, \tag{16}$$

where

$$\mathbf{M}=\begin{bmatrix}\mathbf{Y}_{ma}-\mathbf{Y}_{mb}\mathbf{Y}_{md}^{-1}\mathbf{Y}_{mc} & \mathbf{Y}_{mb}\mathbf{Y}_{md}^{-1}\\ -\mathbf{Y}_{md}^{-1}\mathbf{Y}_{mc} & \mathbf{Y}_{md}^{-1}\end{bmatrix}. \tag{17}$$

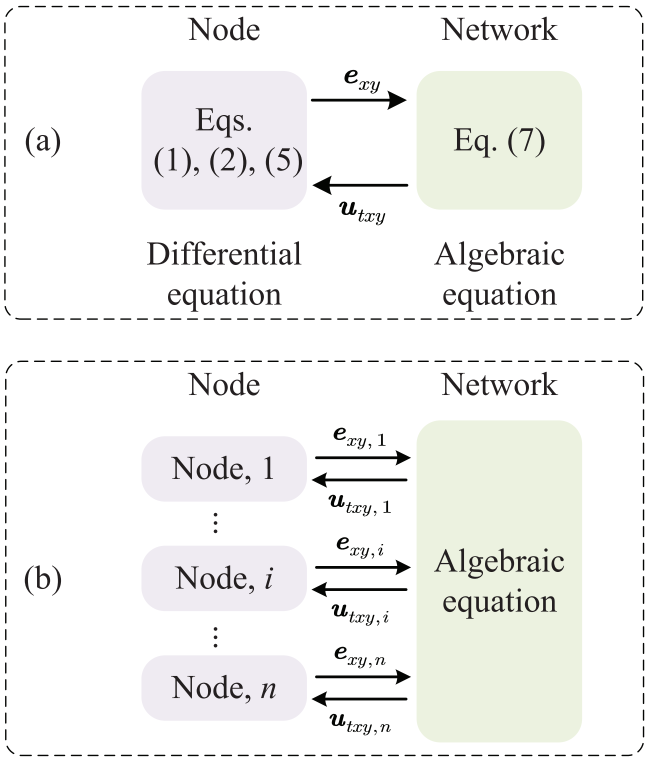

FIG. 12. Differential–algebraic modeling framework of the RDPS within the AC current control timescale for (a) single generator infinite system and (b) multiple generator systems. By using the network algebraization, the node is described by differential equation and the network by the algebraic equation, where the internal voltages e_{xy} and the terminal voltages u_{txy} are chosen as the input–output variables of nodes and networks. Thus, the network for the interaction serves as a steady-state voltage distributor.

In this respect, by separately treating the controlled current and voltage sources for the nodes, we can still describe the network dynamics by modified algebraic equations. By combining the node dynamical model and the quasi-steady network model, we can establish a large-scale nonlinear model of the RDPS within the DC voltage and electromechanical timescales. For more details, see Ref. 56.

B. Dynamical network and algebraization

Next, let us study the dynamical network within the current control timescale. For the single-VSC grid-tied system within this timescale above, we have already known that the dynamics of the filter inductor should be described by differential equations [Eq. (5)], whereas the dynamics of the transmission line inductor can be described by algebraic equations [Eq. (7)], as the dynamical equations of the grid inductor in Eq. (6) is actually superfluous. For the node, it outputs the internal potentials e_{xy} and inputs the terminal voltages u_{txy}, and meanwhile, for the network, it outputs u_{txy} and inputs e_{xy}. The model structure is schematically shown in Fig. 12(a). Therefore, even when the fastest current scale dynamics has to be considered, the DAE description is still available, but in a distinctive form.

Inspired by these results, we can establish a similar model of algebraic equations for a general dynamical network, under the simplified condition that all line resistors and ground capacitors of the transmission lines of the network are neglected. These assumptions are generally reasonable for high voltage transmission scenarios. When the capacitive effects are considered, there are no simple algebraic equations to depict the dynamic network. In this respect, the dynamic network can be described by algebraic equations when the filter inductor dynamics are integrated into the node dynamical equations. Similarly, the whole system can be described by DAEs, where nodes are described by differential equations, and the network is depicted by algebraic equations. With this network algebraization technique, the model has the same precision with the EMT simulations, but is much more computationally efficient. In addition, the interaction relation between nodes and network also becomes clear, namely, the network acts as a voltage divider instantaneously generating terminal voltages (u_{txy}) according to the internal potentials of nodes (e_{xy}). The corresponding model structure is illustrated in Fig. 12(b), which is similar to the traditional electromechanical model. For more details about the multiscale network dynamics, it can be found in the preprint manuscript.[91] Finally, the multi-timescale properties of the network for each timescale are summarized in Table II.

IV. CONCLUSIONS

In conclusion, the synchronization and multi-timescale properties of the RDPS have been systematically studied and summarized for the first time. Multi-scale dynamics of both apparatuses (nodes) and electrical network have been separately considered and analyzed. By getting rid of engineering details, the bulk dynamical behavior within each timescale has been outlined, under the generalized approach that slower dynamics is assumed as unchanged and faster dynamics is believed as damped. Similar to the different-order standard models of the SG,[7–9] a model framework for the RDPS dynamics has been established and relations between different models have been clarified. Our study shows that as the PLL is a nonlinear controller and it plays a key role in all timescale dynamics. Then, the usual synchronization stability mainly restricted within the electromagnetic timescale should be generally observable in the RDPS

TABLE II. Multi-timescale dynamics of the network.

Timescale	Network depiction	Model
DC voltage control and electromechanical timescale	Quasi-steady network	Algebraic equations
AC current control	Dynamic network	Differential equations (algebraic equations by algebraization)

TABLE III. Comparison of synchronization in traditional power system and RDPS.

	Traditional power system	RDPS
Dominating generator	Synchronous generator	Converter-based generator
Synchronization form	Rotor motion	PLL control
Power imbalance object	Rotor	AC filter inductor, DC capacitor, and rotor
Node timescale	Electromechanical	Electromechanical and electromagnetic
Network treatment	Algebraic equations	Algebraic equations and algebraization
Synchronization variable	Rotor angle δ	PLL output angle φ_{pll}
Leading equation	Swing equation	Generalized swing equation

and has a stronger influence than researchers previously thought. For each type of renewable apparatuses, the classification of the slowest timescale and the identification of the associated major controllers, which are summarized in Table I, are significant. With these single-timescale studies, it is also helpful for interaction analysis in the future. For the network analysis, the multiscale separation due to multiscale node dynamics, modified algebraic equations for steady-state network, network algebraization for dynamical network, and universal DAE descriptions for all-timescale network dynamics are also important, as shown in Table II. In addition, the synchronization between the RDPS and the traditional power system is compared under different aspects and summarized in Table III. Clearly, all these findings give a panoramic picture for the RDPS multi-scale dynamics and help us understand its synchronization mechanism better.

V. SOME PERSPECTIVES

Finally, some relevant problems and future works are addressed as follows:

(1) In our recent paper on the understanding of the concept of synchronous stability,[37] we have found that even in transient processes, the PLL apparatus is stable, as the PLL control error is always finite. Therefore, the RDPS synchronization should be understood as the output synchronization between the electrical rotation vectors (φ_{pll}) from each item of the grid-tied apparatus, rather than the synchronization of the PLL apparatus itself. In addition, we have found that the PLL output angle φ_{pll} plays an active role in the system synchronization dynamics and can work as a dominant observable in transient processes; for more details, see Ref. 37. Clearly, for the synchronizations in not only the traditional SG-dominated power system but also the converter-dominated RDPS, which are characterized by the swing of the rotor and the PLL output angle, respectively, they show different patterns. However, they have the same root in the phase-locked synchronization concept in nonlinear sciences for an identical frequency and a constant phase mismatch of coupled subsystems.

(2) For the multi-scale analysis, the well-known Haken's slave principle indicates that the slow-scale factor could always catch the primary system dynamics, whereas the fast-scale factor could damp quickly and play no significant role.[92] Therefore, under the prerequisite that the faster timescale dynamics is stable, the slower timescale dynamics could become crucial. This is clear in Fig. 8. This also fits with the singularity perturbation theory in mathematics. The interaction between different timescales remains to be studied.

(3) In addition to the multiscale cascading controls, switching controls under faults are commonly installed to protect apparatuses and meet grid code during severe faults. In addition, several hardware circuits are installed to release extra power and protect power electronic devices. For instance, in the DFIG, faster PLL control and crowbar circuit are needed to avoid device overcurrent. Within the DC voltage control timescale, the reactive power priority strategy is widely adopted to support the power grid, with a smaller active current reference and a larger reactive current reference. Meanwhile, a chopper circuit is used to avoid over-voltage on the DC capacitor. Correspondingly, within the electromechanical timescale, usually an emergency pitching control is adopted to prevent over-speed of the wind turbine. Thus, under severe faults, fault controls and hardware circuits start to serve under various switch conditions. Clearly, these sequential switching controls make the system dynamics analysis much more complicated. In addition, for any converter, there are always hard-limiters to limit the output values. During severe faults, switching controls and saturations would induce discontinuity and non-smoothness of certain state variables, and this considerably increases the difficulty in theoretical analysis. Until now, the RDPS dynamics studies are extremely dependent on EMT analysis programs. Hence, novel analytical methods to deal with these discontinuous and non-smooth effects are highly appreciated.

(4) For some other fundamental difficulties, the structure and parameters of renewable apparatuses are not fully transparent mostly for the sake of commercial secrecy. For apparatus manufacture companies, they may use different controllers and choose different parameters. To meet the mandatory requirement of grid codes, they may even add some special controllers. Therefore, usually only gray-box or black-box models based on parameter identification methods are used.[93] This certainly brings difficulties in modeling and analysis. In addition, due to the low energy density for renewable energy, the power on individual renewable apparatuses is much lower than that on SGs. Usually, hundreds of renewable apparatuses are integrated to a hub, serving as a farm, and then integrated to the grid. How to

achieve a coordinated operation and control of this large-scale distributed RDPS is a big challenge.

(5) In the traditional power system operation and control, complex system theories, in particular, self-organization criticality and complex network theory, have played a very important role.[94] Power system engineers have been aware of this point in their long-time practices, for example, making the control structure simple, making the administrate organized, controlling the fault evolving direction, dissipating the system entropy promptly, etc.[94] The traditional power system analysis has also benefited a lot from the multi-timescale decomposition principle and under some assumptions and/or approximations. It helps us concentrate on major problems in analysis. The synchronization and multi-scale are common in any large-scale complex system, such as brain[95] and power grid.[7] Due to the intrinsic characteristics of renewable energy apparatuses which is fundamentally different from the SG, the RDPS complexity increases sharply. We like to see that power system engineers can benefit from the complex system theories actively and meanwhile, complex system researchers can have an essential contribution to these emerging hard problems.[35,96]

ACKNOWLEDGMENTS

This work was partially supported by the National Natural Science Foundation of China (NNSFC) under Grant Nos. U22B6008 and 12075091.

AUTHOR DECLARATIONS

Conflict of Interest

The authors have no conflicts to disclose.

Author Contributions

Rui Ma: Conceptualization (equal); Investigation (equal); Methodology (equal); Validation (equal); Visualization (equal); Writing – original draft (equal); Writing – review & editing (equal). **Yayao Zhang:** Conceptualization (equal); Investigation (equal); Methodology (equal); Validation (equal); Visualization (equal); Writing – original draft (equal); Writing – review & editing (equal). **Miao Han:** Conceptualization (equal); Investigation (equal); Methodology (equal); Validation (equal); Visualization (equal); Writing – original draft (equal); Writing – review & editing (equal). **Jürgen Kurths:** Supervision (equal); Writing – review & editing (equal). **Meng Zhan:** Conceptualization (equal); Investigation (equal); Methodology (equal); Supervision (equal); Validation (equal); Visualization (equal); Writing – original draft (equal); Writing – review & editing (equal).

DATA AVAILABILITY

The data that support the findings of this study are available within the article.

APPENDIX A: NOMENCLATURE

Acronym	= Full name
RDPS	= Renewable-dominated power system
DAE	= Differential–algebraic equation
PMSG	= Permanent magnetic synchronous generator
PV	= Photovoltaic
MSC	= Machine-side converter
ACC	= Alternating current control
TVC	= Terminal voltage control
AIC	= Additional inertia control
RPC	= Reactive power control
EMT	= Electromagnetic transient
SG	= Synchronous generator
PWM	= Pulse-width modulation
DFIG	= Double-fed induction generator
VSC	= Voltage source converter
GSC	= Grid-side converter
PLL	= Phase-locked loop
DVC	= Direct voltage control
RSC	= Rotor speed control
MPPT	= Maximum power point tracking
PI	= Proportional integral

Symbol	Physical quantity	Symbol	Physical quantity
xy	Subscript, variables in xy frame	dq	Subscript, variables in dq frame
φ_{pll}	Angle difference between dq and xy frames	x_{pll}	Output of PLL integrator
e_{dq}	dq components of internal voltage	i_{dq}	dq components of current
u_{tdq}	dq components of terminal voltage	U_g	Voltage amplitude of infinite bus
L_f	Filter inductance	L_g	Grid inductance
P_m	Mechanical power from turbine	P_{in}	Injection power from machine side
P_e	Output electromagnetic power	P_s	Stator power of DFIG
P_t	Totally generated power of DFIG	P_{pv}	PV panel power output
u_{pv}	Voltage of PV panel	f_{pv}	Nonlinear function between P_{pv} and u_{pv}
u_{dcref}	Reference of DC voltage	i_{dqref}	References of dq currents
u_{tdref}	Reference of terminal voltage	C_{dc}	DC capacitance
$x_{acc1,2}$	Output of ACC integrator	u_{dc}	DC voltage
x_{tvc}	Output of TVC integrator	x_{dvc}	Output of DVC integrator

Symbol	Physical quantity	Symbol	Physical quantity
$k_{i,acc}$, $k_{p,acc}$	PI parameters of ACC	$k_{i,pll}$, $k_{p,pll}$	PI parameters of PLL
$k_{i,tvc}$, $k_{p,tvc}$	PI parameters of TVC	$k_{i,dvc}$, $k_{p,dvc}$	PI parameters of DVC
K_f, T_f	Control parameters of AIC	H	Inertia constant of generator
$k_{p,rsc}$, $k_{i,rsc}$	PI parameters of RSC	L_{dq}	Stator inductances of PMSG
L_m	Mutual inductance of rotor and stator	L_s	Stator inductance of DFIG
$\mathbf{Y}_r$	Reduced nodal admittance matrix	$\mathbf{M}$	Mixed matrix

APPENDIX B: PARAMETERS USED IN THE SIMULATION

Parameters of the electrical network: $f_0 = 50$ Hz (1.0 p.u.), $\omega_0 = 2\pi f_0$ (1.0 p.u.), $L_f = 0.1$ p.u., $L_g = 0.5$ p.u.

Parameters of the MSC in the PMSG: $P_m = 0.8$ p.u., $L_d = 0.4026$ p.u., $L_q = 0.4903$ p.u., $H = 4$ p.u., $F_r = 0.9$ p.u., $\omega_{rref} = 1$ p.u.; (1) AIC: $K_f = 50$, $T_f = 1$; (2) RSC: $k_{p,rsc} = 15$, $k_{i,rsc} = 50$. (3) ACC: $k_{p,acc} = 0.3$, $k_{i,acc} = 160$.

Parameters of the GSC in the PMSG: (1) DVC: $k_{p,dvc} = 3.5$, $k_{i,acc} = 140$. (2) TVC: $k_{p,tvc} = 1$, $k_{i,tvc} = 100$. (3) ACC: $k_{p,acc} = 0.3$, $k_{i,acc} = 160$. (4) PLL: $k_{p,pll} = 50$, $k_{i,pll} = 2000$.

APPENDIX C: KRON REDUCTION OF NETWORK

In the traditional power system,[7–9] usually the network is described by the nodal admittance matrix

$$\begin{bmatrix} \mathbf{I}_1 \\ \mathbf{0} \end{bmatrix} = \begin{bmatrix} \mathbf{Y}_a & \mathbf{Y}_b \\ \mathbf{Y}_c & \mathbf{Y}_d \end{bmatrix} \begin{bmatrix} \mathbf{U}_1 \\ \mathbf{U}_2 \end{bmatrix}, \tag{C1}$$

where $\mathbf{I}_1$ and $\mathbf{U}_1$ represent the current and voltage vectors of the SG node, respectively, and $\mathbf{U}_2$ denotes the voltage vector of the non-generator nodes, including intermediate nodes and load nodes which can be described by constant impedances. Correspondingly, $\mathbf{Y}_a$, $\mathbf{Y}_b$, $\mathbf{Y}_c$, and $\mathbf{Y}_d$ denote the four components of the node admittance matrix.

Furthermore, by using the classical Kron reduction,[7–9] all non-generator nodes can be eliminated, yielding

$$\mathbf{I}_1 = \mathbf{Y}_r \mathbf{U}_1, \tag{C2}$$

where the reduced admittance matrix $\mathbf{Y}_r$ is

$$\mathbf{Y}_r = \mathbf{Y}_a - \mathbf{Y}_b \mathbf{Y}_d^{-1} \mathbf{Y}_c. \tag{C3}$$

After the Kron reduction, all SGs are directly connected.

APPENDIX D: CLASSICAL MODEL OF SG

For the transient stability analysis of SG systems, usually the classical model of SG is used,[7–9] where the SG is represented by a constant electromotive force E' behind a transient reactance X'_d, and both the magnitude of the transient electromotive force E' and its phase position with respect to the rotor are assumed to be constant. Meanwhile, the rotor transient saliency is neglected. Therefore, the classical swing equation for a single SG tied to an infinite bus can be described by

$$\begin{cases} \dot{\delta} = \omega, \\ M\dot{\omega} = P_m - K \sin\delta - D\omega, \end{cases} \tag{D1}$$

where $K = \frac{EU_g}{X}$ ($E = E'$, $X = X'_d + X_g$ for the sum of the transient reactance X'_d and the transmission line reactance X_g, and U_g denotes the magnitude of the infinite bus), P_m is the mechanical power supplied by a prime mover to the SG, M and D denote the inertia and damping of SG, respectively, and δ ($\delta \approx \delta'$) represents the angle of E with respect to the infinite bus and it also represents the spatial position of rotor of SG. Clearly, it is the same as the second-order Kuramoto phase oscillator model.[6,11–15]

For the N coupled SGs, where each SG is modeled by the classical model, we have the following DAEs:

$$\begin{cases} \dot{\delta}_i = \omega_i, \\ M_i\dot{\omega}_i = P_i - P_{ei} - D\omega_i, \end{cases} \tag{D2}$$

and

$$\begin{cases} P_i = P_{mi} - E_i^2 G_{ii}, \\ P_{ei} = E_i \sum_{j=1}^{n} E_j \left[G_{ij}\cos\left(\delta_i - \delta_j\right) + B_{ij}\sin\left(\delta_i - \delta_j\right) \right], \quad i = 1, \ldots, N \end{cases} \tag{D3}$$

when the loads are established as the constant impedance model and all non-generator nodes are eliminated by the Kron reduction as in Eq. (C2). Here, $\mathbf{Y}_{ij} = G_{ij} + jB_{ij}$ are the elements of the reduced admittance matrix $\mathbf{Y}_r$. Usually, the mechanical power is set as constant, and the electromagnetic power is determined by the angle difference between any two generators. Clearly, both SG nodes and networks are key components in this coupled nonlinear system. It is also similar to the model of coupled second-order Kuramoto phase oscillators.[6,11–15]

It is notable that here only the simplest model of SG, the swing equation, has been introduced. However, it catches the core of rotor synchronization dynamics under power imbalance for the slowest dynamics. For engineering practice, there are many higher order models to accurately catch the dynamics of the SG and the SG-dominated traditional power system, such as different forms of electromotive force with associated reactances, salient effect of rotor, excitation systems, automatic voltage regulators, power system stabilizer, etc.[7–9] It is indisputable that as the SG is the heart of the traditional power system, its dynamical performance is top priority. For more details, see any classical textbook on power system dynamics, stability/control, or analysis.[7–9]

REFERENCES

[1] S. H. Strogatz, *Sync: How Order Emerges from Chaos in the Universe, Nature, and Daily Life* (Hachette, 2012).
[2] A. S. Pikovsky, M. G. Rosenblum, and J. Kurths, *Synchronization: A Universal Concept in Nonlinear Science* (Cambridge University Press, 2001).
[3] P. Ji, T. K. D. Peron, P. J. Menck, F. A. Rodrigues, and J. Kurths, "Cluster explosive synchronization in complex networks," Phys. Rev. Lett. **110**, 218701 (2013).
[4] S. Su, J. Xiao, W. Liu, and Y. Wu, "Synchronization mechanism of clapping rhythms in mutual interacting individuals," Chin. Phys. B **30**, 010505 (2021).
[5] A. Gajduk, M. Todorovski, and L. Kocarev, "Stability of power grids: An overview," Eur. Phys. J. Spec. Top. **223**, 2387–2409 (2014).
[6] S. H. Strogatz, *Nonlinear Dynamics and Chaos: With Applications to Physics, Biology, Chemistry, and Engineering* (Westview Press, 2015).
[7] P. Kundur, *Power System Stability and Control* (McGraw-Hill, 1994).
[8] P. M. Anderson and A. A. Fouad, *Power System Control and Stability* (The Iowa State University Press, 1994).
[9] J. Machowski, Z. Lubosny, J. W. Bialek, and J. R. Bumby, *Power System Dynamics: Stability and Control* (John Wiley & Sons, 2020).
[10] C. Concordia, *Synchronous Machines. Theory and Performance* (John Wiley & Sons, New York, 1951).
[11] D. Skubov, A. Lukin, and I. Popov, "Bifurcation curves for synchronous electrical machine," Nonlinear Dyn. **83**, 2323–2329 (2016).
[12] M. Sarkar and S. Gupta, "Synchronization in the Kuramoto model in presence of stochastic resetting," Chaos **32**, 073109 (2022).
[13] F. Rodrigues, T. Peron, P. Ji, and J. Kurths, "The Kuramoto model in complex networks," Phys. Rep. **610**, 1–98 (2016).
[14] J. Grzybowski, E. Macau, and T. Yoneyama, "On synchronization in power-grids modelled as networks of second-order Kuramoto oscillators," Chaos **26**, 113113 (2016).
[15] D. Subbarao and K. Singh, "Hysteresis and bifurcations in the classical model of generator," IEEE Trans. Power Syst. **19**, 1918–1924 (2004).
[16] G. Filatrella, A. H. Nielsen, and N. F. Pedersen, "Analysis of a power grid using a Kuramoto-like model," Eur. Phys. J. B **61**, 485–491 (2008).
[17] J. A. Acebrón, L. L. Bonilla, C. J. P. Vicente, F. Ritort, and R. Spigler, "The Kuramoto model: A simple paradigm for synchronization phenomena," Rev. Mod. Phys. **77**, 137 (2005).
[18] D. Witthaut, F. Hellmann, J. Kurths, S. Kettemann, H. Meyer-Ortmanns, and M. Timme, "Collective nonlinear dynamics and self-organization in decentralized power grids," Rev. Mod. Phys. **94**, 015005 (2022).
[19] S. Liu and C. Chen, *Energy Function Analysis for Power System Transient Stability—Network Structure Preserving Model* (Science Press, 2014) (in Chinese).
[20] Y. Xue, T. Van Cutsem, and M. Ribbens-Pavella, "A simple direct method for fast transient stability assessment of large power systems," IEEE Trans. Power Syst. **3**, 400–412 (1988).
[21] H.-D. Chiang, C.-C. Chu, and G. Cauley, "Direct stability analysis of electric power systems using energy functions: Theory, applications, and perspective," Proc. IEEE **83**, 1497–1529 (1995).
[22] H.-D. Chiang, F. Wu, and P. Varaiya, "Foundations of direct methods for power system transient stability analysis," IEEE Trans. Circuits Syst. **34**, 160–173 (1987).
[23] F. Blaabjerg, Y. Yang, K. A. Kim, and J. Rodriguez, "Power electronics technology for large-scale renewable energy generation," Proc. IEEE **111**, 335–355 (2023).
[24] Z. Tang, Y. Yang, and F. Blaabjerg, "Power electronics: The enabling technology for renewable energy integration," CSEE J. Power Energy Syst. **8**, 39–52 (2022).
[25] X. Yuan, J. Hu, and S. Cheng, "Multi-time scale dynamics in power electronics-dominated power systems," Front. Mech. Eng. **12**, 303–311 (2017).
[26] R. Ma, Z. Yang, S. Cheng, and M. Zhan, "Sustained oscillations and bifurcations in three-phase voltage source converters tied to AC gird," IET Renew. Power Gen. **14**, 3770–3781 (2020).
[27] H. Yuan, X. Yuan, and J. Hu, "Modeling of grid-connected VSCs for power system small-signal stability analysis in DC-link voltage control timescale," IEEE Trans. Power Syst. **32**, 3981–3991 (2017).
[28] W. Tang, J. Hu, Y. Chang, and F. Liu, "Modeling of DFIG-based wind turbine for power system transient response analysis in rotor speed control timescale," IEEE Trans. Power Syst. **33**, 6795–6805 (2018).
[29] Y. Chang, J. Hu, W. Tang, and G. Song, "Fault current analysis of type-3 WTs considering sequential switching of internal control and protection circuits in multi time scales during LVRT," IEEE Trans. Power Syst. **33**, 6894–6903 (2018).
[30] Y. Ma, D. Zhu, Z. Zhang, X. Zou, J. Hu, and Y. Kang, "Modeling and transient stability analysis for type-3 wind turbines using singular perturbation and Lyapunov methods," IEEE Trans. Ind. Electron. **70**, 8075–8086 (2022).
[31] K. T. Chi, M. Huang, X. Zhang, D. Liu, and X. L. Li, "Circuits and systems issues in power electronics penetrated power grid," IEEE Open J. Circ. Syst. **1**, 140–156 (2020).
[32] Q. Jiang and C. Zhao, "Electromagnetic transient synchronization stability issue of grid-connected inverters," J. Tsinghua Univ. **21**, 1–14 (2021) (in Chinese).
[33] Y. Zhang, X. Cai, C. Zhang, J. Lyu, and Y. Li, "Transient synchronization stability analysis of voltage source converters: A review," Proc. CSEE **41**, 1687–1701 (2021) (in Chinese).
[34] H. Geng, C. He, Y. Liu, X. He, and M. Li, "Overview on transient synchronization stability of renewable-rich power systems," High Voltage Eng. **48**, 3367–3383 (2022) (in Chinese).
[35] R. Ma, Y. Zhang, Z. Yang, J. Kurths, M. Zhan, and C. Lin, "Synchronization stability of power-grid-tied converters," Chaos **33**, 032102 (2023).
[36] X. Wang, M. G. Taul, H. Wu, Y. Liao, F. Blaabjerg, and L. Harnefors, "Grid-synchronization stability of converter-based resources—an overview," IEEE Open J. Ind. Appl. **1**, 115–134 (2020).
[37] Y. Zhang, M. Han, and M. Zhan, "The concept and understanding of synchronous stability in power-electronic-based power systems," Energies **16**, 2923 (2023).
[38] Y. Gu and T. C. Green, "Power system stability with a high penetration of inverter-based resources," Proc. IEEE **111**, 832–853 (2022).
[39] Y. Li, Y. Gu, and T. C. Green, "Revisiting grid-forming and grid-following inverters: A duality theory," IEEE Trans. Power Syst. **37**, 4541–4554 (2022).
[40] D. Dong, B. Wen, D. Boroyevich, P. Mattavelli, and Y. Xue, "Analysis of phase-locked loop low-frequency stability in three-phase grid-connected power converters considering impedance interactions," IEEE Trans. Ind. Electron. **62**, 310–321 (2014).
[41] X. Fu, M. Huang, C. K. Tse, J. Yang, Y. Ling, and X. Zha, "Synchronization stability of grid-following VSC considering interactions of inner current loop and parallel-connected converters," IEEE Trans. Smart Grid (published online 2023).
[42] N. Hatziargyriou, J. Milanović, C. Rahmann, V. Ajjarapu, C. Cañizares, I. Erlich, D. Hill, I. Hiskens, I. Kamwa, B. Pal *et al.*, "Stability definitions and characterization of dynamic behavior in systems with high penetration of power electronic interfaced technologies," IEEE PES Technical Report PES-TR77 (2020).
[43] M. Huang, Y. Peng, C. Tse, Y. Liu, J. Sun, and X. Zha, "Bifurcation and large-signal stability analysis of three-phase voltage source converter under grid voltage dips," IEEE Trans. Power Electron. **32**, 8868–8879 (2017).
[44] Z. Yang, R. Ma, S. Cheng, and M. Zhan, "Nonlinear modeling and analysis of grid-connected voltage-source converters under voltage dips," IEEE J. Emerg. Select. Top. Power Electron. **8**, 3281–3292 (2020).
[45] M. He, W. He, J. Hu, X. Yuan, and M. Zhan, "Nonlinear analysis of a simple amplitude–phase motion equation for power-electronics-based power system," Nonlinear Dyn. **95**, 1965–1976 (2019).
[46] Q. Hu, L. Fu, F. Ma, and F. Ji, "Large signal synchronizing instability of PLL-based VSC connected to weak AC grid," IEEE Trans. Power Syst. **34**, 3220–3229 (2019).
[47] R. Ma, J. Li, J. Kurths, S. Cheng, and M. Zhan, "Generalized swing equation and transient synchronous stability with PLL-based VSC," IEEE Trans. Energy Convers. **37**, 1428–1441 (2022).
[48] X. Fu, J. Sun, M. Huang, Z. Tian, H. Yan, H. H.-C. Iu, P. Hu, and X. Zha, "Large-signal stability of grid-forming and grid-following controls in voltage source converter: A comparative study," IEEE Trans. Power Electron. **36**, 7832–7840 (2021).

[49] C. Zhang, X. Cai, A. Rygg, and M. Molinas, "Modeling and analysis of grid-synchronizing stability of a type-IV wind turbine under grid faults," Int. J. Electr. Power Energy Syst. **117**, 105544 (2020).
[50] Y. Zhang, C. Zhang, and X. Cai, "Large-signal grid-synchronization stability analysis of PLL-based VSCs using Lyapunov's direct method," IEEE Trans. Power Syst. **37**, 788–791 (2022).
[51] Z. Zhang, R. Schuerhuber, L. Fickert, K. Friedl, G. Chen, and Y. Zhang, "Domain of attraction's estimation for grid connected converters with phase-locked loop," IEEE Trans. Power Syst. **37**, 1351–1362 (2022).
[52] H. Wu and X. Wang, "Design-oriented transient stability analysis of PLL-synchronized voltage-source converters," IEEE Trans. Power Electron. **35**, 3573–3589 (2020).
[53] M. Zarif Mansour, S. Me, S. Hadavi, B. Badrzadeh, A. Karimi, and B. Bahrani, "Nonlinear transient stability analysis of phased-locked loop based grid-following voltage source converters using Lyapunov's direct method," IEEE J. Emerg. Select. Top. Power Electron. **10**, 2699–2709 (2022).
[54] J. Zhao, M. Huang, and X. Zha, "Nonlinear analysis of PLL damping characteristics in weak-grid-tied inverters," IEEE Trans. Circ. Syst. II: Express Briefs **67**, 2752–2756 (2020).
[55] W. Wang, G. Huang, D. Ramasubramanian, and E. Farantatos, "Transient stability analysis and stability margin evaluation of phase-locked loop synchronised converter-based generators," IET Gen. Transm. Distrib. **14**, 5000–5010 (2020).
[56] Z. Yang, M. Zhan, D. Liu, C. Ye, K. Cao, and S. Cheng, "Small-signal synchronous stability of a new-generation power system with 100% renewable energy," IEEE Trans. Power Syst. (published online 2022).
[57] X. Fu, M. Huang, S. Pan, and X. Zha, "Cascading synchronization instability in multi-VSC grid-connected system," IEEE Trans. Power Electron. **37**, 7572–7576 (2022).
[58] M. Taul, X. Wang, P. Davari, and F. Blaabjerg, "Reduced-order and aggregated modeling of large-signal synchronization stability for multi-converter systems," IEEE J. Emerg. Select. Top. Power Electron. **9**, 3150–3165 (2021).
[59] D. Pal and B. K. Panigrahi, "Reduced-order modeling and transient synchronization stability analysis of multiple heterogeneous grid-tied inverters," IEEE Trans. Power Delivery **38**, 1074–1085 (2022).
[60] Y. Zhou, J. Hu, and W. He, "Synchronization mechanism between power-synchronized VS and PLL-controlled CS and the resulting oscillations," IEEE Trans. Power Syst. **37**, 4129–4132 (2022).
[61] A. Sajadi, R. Kenyon, and B.-M. Hodge, "Synchronization in electric power networks with inherent heterogeneity up to 100% inverter-based renewable generation," Nat. Commun. **13**, 2490 (2022).
[62] D. Lew, D. Bartlett, A. Groom *et al.*, "Getting to 100% renewables: Operating experiences with very high penetrations of variable energy resources," IET Renew. Power Gen. **14**, 3899–3907 (2020).
[63] X. Zhao, P. Thakurta, and D. Flynn, "Grid-forming requirements based on stability assessment for 100% converter-based Irish power system," IET Renew. Power Gen. **16**, 447–458 (2022).
[64] W. Tang, B. Zhou, J. Hu, Z. Guo, and R. Zhang, "Transient synchronous stability of PLL-based wind power-synchronous generation interconnected power system in rotor speed control timescale," Proc. CSEE **41**, 6900–6915 (2021) (in Chinese).
[65] Y. Chi, B. Tang, J. Hu, X. Tian, H. Tang, Y. Li, S. Sun, L. Shi, and L. Shuai, "Overview of mechanism and mitigation measures on multi-frequency oscillation caused by large-scale integration of wind power," CSEE J. Power Energy Syst. **5**, 433–443 (2019).
[66] X. Yang, R. Ma, and M. Zhan, "Dynamic and static network analysis and power transmission characteristics of power system oscillations," Proc. CSEE (published online 2022) (in Chinese).
[67] J. Vega-Herrera, C. Rahmann, F. Valencia, and K. Strunz, "Analysis and application of quasi-static and dynamic phasor calculus for stability assessment of integrated power electric and electronic systems," IEEE Trans. Power Syst. **36**, 1750–1760 (2021).
[68] N. Pogaku, M. Prodanovic, and T. C. Green, "Modeling, analysis and testing of autonomous operation of an inverter-based microgrid," IEEE Trans. Power Electron. **22**, 613–625 (2007).
[69] H. Yang and X. Yuan, "Modeling and analyzing the effect of frequency variation on weak grid-connected VSC system stability in DC voltage control timescale," Energies **12**, 4458 (2019).
[70] Y. Ji, W. He, S. Cheng, J. Kurths, and M. Zhan, "Dynamic network characteristics of power-electronics-based power systems," Sci. Rep. **10**, 9946 (2020).
[71] Z. Yang, J. Yu, J. Kurths, and M. Zhan, "Nonlinear modeling of multi-converter systems within DC-link timescale," IEEE J. Emerg. Select. Top. Circ. Syst. **11**, 5–16 (2021).
[72] A. Yazdani and R. Iravani, *Voltage-Sourced Converters in Power Systems: Modeling, Control, and Applications* (John Wiley & Sons, 2010).
[73] S. Bacha, I. Munteanu, and A. I. Bratcu, *Power Electronic Converters Modeling and Control* (Springer, 2014).
[74] J. Chen, M. Liu, T. O'Donnell, and F. Milano, "Impact of current transients on the synchronization stability assessment of grid-feeding converters," IEEE Trans. Power Syst. **35**, 4131–4134 (2020).
[75] Q. Hu, L. Fu, F. Ma, F. Ji, and Y. Zhang, "Analogized synchronous-generator model of PLL-based VSC and transient synchronizing stability of converter dominated power system," IEEE Trans. Sustain. Energy **12**, 1174–1185 (2020).
[76] X. Yuan, S. Cheng, and J. Hu, "Multi-time scale voltage and power angle dynamics in power electronics dominated large power systems," Proc. CSEE **36**, 5145–5154 (2016) (in Chinese).
[77] R. Ma, Q. Qiu, J. Kurths, and M. Zhan, "Fast-slow-scale interaction induced parallel resonance and its suppression in voltage source converters," IEEE Access **9**, 90126–90141 (2021).
[78] W. Du, Y. Wang, H. Wang, B. Ren, and X. Xiao, "Small-disturbance stability limit of a grid-connected wind farm with PMSGs in the timescale of DC voltage dynamics," IEEE Trans. Power Syst. **36**, 2366–2379 (2020).
[79] M. G. Taul, C. Wu, S.-F. Chou, and F. Blaabjerg, "Optimal controller design for transient stability enhancement of grid-following converters under weak-grid conditions," IEEE Trans. Power Electron. **36**, 10251–10264 (2021).
[80] X. He, H. Geng, and G. Mu, "Modeling of wind turbine generators for power system stability studies: A review," Renew. Sustain. Energy Rev. **143**, 110865 (2021).
[81] K. Clark, N. W. Miller, and J. J. Sanchez-Gasca, "Modeling of GE wind turbine-generators for grid studies," GE Energy Technical Report (2010).
[82] N. Ding, Z. Lu, Y. Qiao, and Y. Min, "Simplified equivalent models of large-scale wind power and their application on small-signal stability," J. Mod. Power Syst. Clean Energy **1**, 58–64 (2013).
[83] Y. Chi, H. Tang, W. Shi, and Y. Li, *Modeling and Grid Integration Analysis of New Energy Generation* (China Electric Power Press, 2019) (in Chinese).
[84] D. Duckwitz and B. Fischer, "Modeling and design of df/dt-based inertia control for power converters," IEEE J. Emerg. Select. Top. Power Electron. **5**, 1553–1564 (2017).
[85] C. Ge, M. Liu, and J. Chen, "Modeling of direct-drive permanent magnet synchronous wind power generation system considering the power system analysis in multi-timescales," Energies **15**, 7471 (2022).
[86] B. Wu, Y. Lang, N. Zargari, and S. Kouro, *Power Conversion and Control of Wind Energy Systems* (John Wiley & Sons, 2011), p. 66.
[87] N. Miller, J. Sanchez-Gasca, W. Price, and R. Delmerico, "Dynamic modeling of GE 1.5 and 3.6 MW wind turbine-generators for stability simulations," in *2003 IEEE Power Engineering Society General Meeting* (IEEE, 2003), Vol. 3, pp. 1977–1983.
[88] O. C. Zevallos, J. B. Da Silva, F. Mancilla-David, F. A. Neves, R. C. Neto, and R. B. Prada, "Control of photovoltaic inverters for transient and voltage stability enhancement," IEEE Access **9**, 44363–44373 (2021).
[89] O. Gandhi, D. S. Kumar, C. D. Rodríguez-Gallegos, and D. Srinivasan, "Review of power system impacts at high PV penetration Part I: Factors limiting PV penetration," Sol. Energy **210**, 181–201 (2020).
[90] M. Yu, W. Huang, N. Tai, X. Xi, and M. H. Nadeem, "Adaptive control scheme based on transient stability mechanism for photovoltaic plants," IET Gen. Trans. Distrib. **14**, 5011–5019 (2020).
[91] R. Ma, X. Yang, and M. Zhan, "Network algebraization and port relationship for power-electronic-dominated power systems," arXiv:2304.09528 [eess.SY] (2023).
[92] H. Haken, *Synergetics: Introduction and Advanced Topics* (Springer, Berlin, 2004).

[93]Q. Qiu, Y. Huang, R. Ma, J. Kurths, and M. Zhan, "Black-box impedance prediction of grid-tied VSCs under variable operating conditions," IEEE Access **10**, 1289–1304 (2021).
[94]M. Li, *Thoughts on Operation and Control Methodology of Power Systems* (STATE GRID Corporation of China, Xi'an, 2023), see https://mp.weixin.qq.com/s/UxKsyDUQQ-xxNiqId4ZPpQ.
[95]C. Presigny and F. D. V. Fallani, "Colloquium: Multiscale modeling of brain network organization," Rev. Mod. Phys. **94**, 031002 (2022).
[96]Z. Yang, R. Ma, S. Cheng, and M. Zhan, "Problems and challenges of power-electronic-based power system stability: A case study of transient stability comparison," Acta Phys. Sin. **69**, 103–116 (2020) (in Chinese).